PEEC Modeling of Radiation Problems for Microstrip Structures

Lap K. Yeung, *Member, IEEE*, and Ke-Li Wu, *Fellow, IEEE*

***Abstract*—In this work, an accurate radiation model for the partial element equivalent circuit (PEEC) technique is introduced for modeling of microstrip structures. By making use of the concept of generalized complex inductance proposed recently for the free-space case, an accurate decomposition of the radiation resistance for a small dipole on microstrip substrate is derived for the first time using PEEC. Using the semi-analytical Green's functions for microstrip substrates, the imaginary part of this complex inductance can be shown to represent a frequency-dependent resistance containing contributions from spatial radiations (spherical and lateral) and surface waves (cylindrical). Hence, depending on how the structure of interest is divided into meshes, an equivalent circuit network of "distributed" radiation resistances can be obtained. Two numerical examples have been carried out to validate the model. Results obtained are in good agreement with those from commercial full-wave electromagnetic (EM) solvers, showing the potential of the proposed model for representing high-speed/high-frequency microstrip structures and antennas in the network realm.**

***Index Terms*—Antennas, microstrip structures, partial element equivalent circuit, radiation resistance.**

I. Introduction

As the data rate increases to multiple gigabits per second in modern digital communication systems, the correct prediction of various electrical performances, e.g., crosstalk interference and signal integrity, for printed circuit board layouts, bonding wires and other types of interconnects becomes more and more critical to designers. At the same time, the design of integrated antennas requires a good understanding of the influence from their surroundings. In order to accurately model different electrical effects, a full-wave description of the electromagnetic (EM) wave phenomena is essential, especially in high-speed and high-frequency cases.

Nowadays, a variety of numerical methods exists for modeling electromagnetic (EM) phenomena, such as method of moments (MoM), finite-difference time-domain (FDTD) method, and finite-element method (FEM). Among all existing methods, the partial element equivalent circuit (PEEC) technique [1] is very popular for modeling of packaging related problems [2]–[8] such as electromagnetic compatibility (EMC), electromagnetic interference (EMI), as well as signal integrity (SI) for high-speed electronic circuits. The major reason for its attractiveness is that it converts a physical layout to a mesh-dependent lumped-element causal circuit network (if the layout is meshed fine enough), which can easily be integrated with other circuit models and solved by conventional circuit solvers. Through the development in the past two decades, the PEEC technique has been evolving to a practical numerical technique for solving more and more complex problems. In fact, this combined circuit and electromagnetic approach also makes itself an attractive tool for antenna analysis and design as it can offer a circuit representation of an antenna and is convenient for conducting system-level simulations.

The existing full-wave PEEC models use time-retarded control sources [9]–[14]. When a retarded control source is used between two capacitive cells, the corresponding equivalent mutual capacitance becomes frequency dependent. It means that the field defining the capacitance is not conservative. Recently, a rigorous radiation model for the PEEC modeling of free-space problems in frequency domain has been proposed [15]. By introducing the concept of generalized complex inductance, the conservative condition of the resultant capacitance matrix is preserved. It has been proven in [15] that when the free-space Green's function (GF) is adopted in the formulation, the generalized complex inductance can exactly account for the radiation effect of electrically small structures. Since the radiation mechanism of a microstrip substrate is intricate, a good understanding of the radiation characteristics of a microstrip dipole would be significant from both academic and practical points of view.

PEEC (or MoM) modeling of microstrip structures using multilayered Green's functions has been done in the past [16], [17]. The major advantage of using such Green's functions is that there is no need to discretize and model the dielectric substrate explicitly. In this paper, the attention is focused on finding the radiation mechanism (in terms of resistances) of microstrip circuits and antennas based on the principle presented in [15]. By using the Green's functions for microstrip substrates, it can be shown that the imaginary part of the inductance represents a frequency-dependent resistance containing contributions from quasi-static images, surface waves and other higher-order effects. Notice that the resulting equivalent circuits employing this complex inductance concept require no "nonconservative" capacitors and the static condition for the capacitive components is thus preserved. Moreover, these equivalent circuits can provide insights to the structures being modeled. In the

Manuscript received July 20, 2012; revised January 22, 2013; accepted March 09, 2013. Date of publication March 26, 2013; date of current version July 01, 2013. This work was supported in part by the University Grants Committee of Hong Kong under Grant AoE/P-04/08 and in part by the Innovation Technology Commission of Hong Kong under Grant ITS/019/10.

The authors are with the Department of Electronic Engineering, The Chinese University of Hong Kong, Shatin, NT, Hong Kong (e-mail: lkyeung@msn.com; klwu@ee.cuhk.edu.hk).

Color versions of one or more of the figures in this paper are available online at http://ieeexplore.ieee.org.

Digital Object Identifier 10.1109/TAP.2013.2254691

following, the generalized inductance concept is developed for the multilayered substrate in general, and for the single-layered microstrip substrate in particular. Two numerical examples are provided to validate the concept.

II. Theory

A. Equivalent Circuit Formulation

The partial element equivalent circuit technique is based on the concept of converting the mixed potential integral equation (MPIE) to a network representation that is suitable for being solved in the circuit domain. By using a specific meshing scheme, a multiconductor structure can be converted to a network consisting of discrete resistances, inductances, as well as capacitances, which are called partial elements. These partial elements compose an electromagnetically accurate equivalent circuit model in which additional components, such as transistor circuit models, can easily be added in. The partial elements are first calculated by using either numerical integration procedures or analytical closed-form formulas. Then, the overall equivalent circuit is solved by a conventional circuit solver.

The frequency-domain PEEC model starts from the MPIE

$$\mathbf{E}(\mathbf{r}) = -j\omega \int_{V'} \bar{\bar{G}}_A(\mathbf{r},\mathbf{r}') \cdot \mathbf{J}(\mathbf{r}')dv' - \nabla \int_{V'} G_\phi(\mathbf{r},\mathbf{r}')\rho(\mathbf{r}')dv', \quad (1)$$

where $\bar{\bar{G}}_A$ and G_ϕ are the dyadic and scalar Green's functions for magnetic vector and electric scalar potentials, respectively. In this particular work, only single-layered microstrip structures with infinitely thin conducting strips are considered. In such case, the volume integrals in (1) should change to surface integrals, and $\mathbf{J}$ and ρ become the surface current and charge densities, respectively. In addition, without loss of generality, only the x-component in (1) is considered. By separately discretizing the current and charge densities using rectangular pulse functions, and having $\mathbf{r}$ resided on the conducting strips, the discretized form of (1) is given by

$$\frac{J_x(\mathbf{r})}{\sigma} = -j\omega \sum_m \left(\int_{S'_m} G_A^{xx}(\mathbf{r},\mathbf{r}')ds'_m \right) J_x^m - \frac{d}{dx} \sum_n \left(\int_{S'_n} G_\phi(\mathbf{r},\mathbf{r}')ds'_n \right) \rho_n. \quad (2)$$

from which a system of M equations is obtained by performing the Galerkin's matching procedure on (2) as

$$\frac{l_l}{\sigma w_l} I_x^l + \sum_m \frac{j\omega}{w_l w_m} \left(\iint G_A^{xx} ds'_m ds_l \right) I_x^m + \sum_n \frac{d}{dx} \frac{1}{w_l a_n} \left(\iint G_\phi ds'_n ds_l \right) Q_n = 0 \quad (3)$$

for $l = 1 \ldots M$ where M is the number of inductive meshes. Notice that those pulse functions used for discretizing the current density are chosen to be the testing functions in this matching operation. Moreover, the integration domains and the arguments inside the Green's functions have been dropped for clarity. Whereas symbols w_l and w_m are the widths of inductive meshes l and m respectively, a_n is the area of capacitive mesh n. It is worth to mention that (3) is in the form of Kirchhoff's voltage law (KVL). The terms on the LHS represents, respectively, the resistive, inductive, and capacitive voltage drops across the matched inductive mesh l. In a more circuit-oriented form, (3) can be represented as (subscript x is dropped from now on)

$$R_l I_l + \sum_m j\omega L_{l,m} I_m + \sum_n \left(pp_{l,n}^+ - pp_{l,n}^- \right) Q_n = 0 \quad (4)$$

where a finite-difference approximation has been used for the derivative operation appearing at the last term. In the following subsections, a generalized $L_{l,m}$ and $pp_{l,n}$ will be developed such that the radiation effect for single-layered microstrip structures can be analyzed in an intuitive way.

B. Single-Layered Microstrip Green's Functions

The rigorous form of magnetic vector and electric scalar Green's functions for microstrip structures are usually expressed in terms of Sommerfeld integral as

$$G = \int \tilde{G}(k_\rho) H_0^{(2)}(k_\rho \rho) k_\rho dk_\rho \quad (5)$$

where $\tilde{G} = \tilde{G}_A^{xx}$ or $\tilde{G}_\phi$ is the corresponding Green's function in the spectral domain, and $H_0^{(2)}$ is the Hankel function of the second kind. In order to compute this integral, a variety of techniques [18]–[22] can be used. In general, for a single-layered microstrip substrate, the two spectral-domain Green's functions can be decomposed into three parts as

$$\tilde{G} = \tilde{G}_0 + \tilde{G}_{\mathrm{SW}} + \frac{F}{j2k_{z0}}. \quad (6)$$

Notice that $k_{z0}^2 = k_0^2 - k_\rho^2$. The first two terms in (6) represent, respectively, the asymptotic ($k_\rho \to \infty$) and surface-wave components of the Green's function. The last term F is the "leftover" for which the first two components do not cover. From the analysis given in [23], the quasi-dynamic terms of the two Green's functions are defined by

$$\tilde{G}_{A0}^{xx} = \frac{\mu_0}{4\pi} \frac{1}{j2k_{z0}} \left[e^{-jk_{z0}(z-z')} - e^{-j2k_{z0}h} e^{-jk_{z0}(z+z')} \right] \quad (7a)$$

$$\tilde{G}_{\phi 0} = \frac{1}{4\pi\varepsilon_0} \frac{1}{j2k_{z0}} \left[e^{-jk_{z0}(z-z')} - e^{-j2k_{z0}h} e^{-jk_{z0}(z+z')} + \frac{K(1-e^{-j4k_{z0}h})}{1-Ke^{-j2k_{z0}h}} e^{-jk_{z0}(z+z')} \right] \quad (7b)$$

with $K = (1-\varepsilon_r)/(1+\varepsilon_r)$ and h is the substrate thickness (see Fig. 1), and the contribution from surface waves are given by

$$\tilde{G}_{A,\mathrm{SW}}^{xx} = \sum_i \frac{2k_{\rho i}\mathrm{Res}_i^A}{k_\rho^2 - k_{\rho i}^2} \quad (8a)$$

$$\tilde{G}_{\phi,\mathrm{SW}} = \sum_i \frac{2k_{\rho i}\mathrm{Res}_i^\phi}{k_\rho^2 - k_{\rho i}^2} \quad (8b)$$

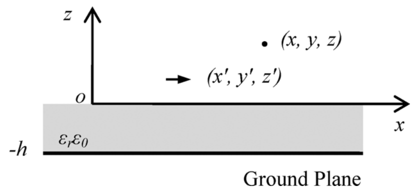

Fig. 1. Single-layered microstrip substrate.

where Res_i^A and Res_i^ϕ are the residues of $\tilde{G}_A^{xx}$ and $\tilde{G}_\phi$ at pole $k_{\rho i}$, respectively. With the analytical expressions listed in (7) and (8), the "leftover" terms for the two Green's functions, F_A^{xx} and F_ϕ, can be obtained.

In this work, the asymptotic and the "leftover" components are considered together as they both contribute to radiations into free space. In this sense, (6) should be rewritten as

$$\tilde{G} = \left(\tilde{G}_0 + \frac{F}{j2k_{z0}}\right) + \tilde{G}_{\mathrm{SW}} = \tilde{G}_{SP} + \tilde{G}_{\mathrm{SW}}. \tag{9}$$

To obtain the corresponding spatial domain Green's functions, the inverse Hankel transform can be performed to (9). However, for the asymptotic scalar Green's function given in (7b), an approximation should first be carried out using

$$\frac{K(1-e^{-j4k_{z0}h})}{1-Ke^{-j2k_{z0}h}} \approx K(1-e^{-j4k_{z0}h}) \times (1+Ke^{-j2k_{z0}h}+\cdots) \tag{10}$$

so that the function can now be rewritten as

$$\tilde{G}_{\phi 0} \approx \frac{1}{4\pi\varepsilon_0}\frac{1}{j2k_{z0}}\Big[e^{-jk_{z0}(z-z')} - e^{-j2k_{z0}h}e^{-jk_{z0}(z+z')} + K(1-e^{-j4k_{z0}h})(1+Ke^{-j2k_{z0}h}+\cdots)e^{-jk_{z0}(z+z')}\Big]. \tag{11}$$

Notice that (11) is not equal to (7b) when the infinite series is truncated and the error introduced in this approximation will be automatically compensated by the "leftover" term. When expanding the last term in (11), the quasi-static images in the spatial domain are found out to be locating at $-z' - 2nh$ for $n = 0, 1, 2\ldots$

By making use of the Sommerfeld identity and Cauchy's integral formula, the spatial-domain Green's functions are given by

$$G_{A,\mathrm{SP}}^{xx} = \frac{\mu_0}{4\pi}\left(\frac{e^{-jk_0 r}}{r} - \frac{e^{-jk_0 r_1}}{r_1}\right) + \int \frac{F_A^{xx}k_\rho}{j2k_{z0}} H_0^{(2)}(k_\rho \rho)dk_\rho \tag{12a}$$

$$G_{\phi,\mathrm{SP}} = \frac{1}{4\pi\varepsilon_0}\left[\frac{e^{-jk_0 r}}{r} + K\frac{e^{-jk_0 r_0}}{r_0} + \sum_n K^{n-1}(K^2-1)\frac{e^{-jk_0 r_n}}{r_n}\right] + \int \frac{F_\phi k_\rho}{j2k_{z0}} H_0^{(2)}(k_\rho\rho)dk_\rho, \tag{12b}$$

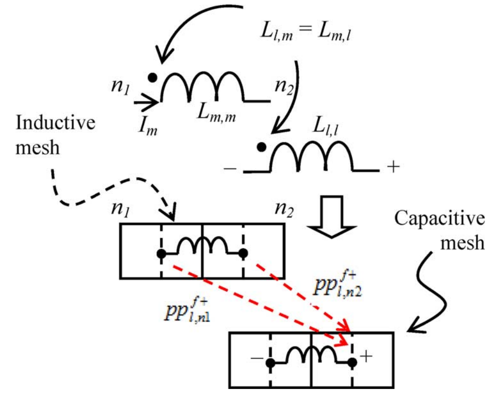

Fig. 2. Coupling configuration between inductors l and m.

where $r_n^2 = \rho^2 + (z + z' + 2\,nh)^2$; together with

$$G_{A,\mathrm{SW}}^{xx} = (-j2\pi)\sum_i \mathrm{Res}_i^A H_0^{(2)}(k_{\rho i}\rho)k_{\rho i} \tag{13a}$$

$$G_{\phi,\mathrm{SW}} = (-j2\pi)\sum_i \mathrm{Res}_i^\phi H_0^{(2)}(k_{\rho i}\rho)k_{\rho i}. \tag{13b}$$

These spatial-domain functions will be used in the partial element calculations. Notice that many methods have been proposed to approximately compute the integrals in (12), in this work, numerical integration is used to avoid any possible errors.

C. Static Capacitance

Following the discussion earlier, the third term in (4) represents the potential difference between the two ends of inductive mesh l (or the two capacitive meshes associated with these two ends) induced by all charges (see Fig. 2). In principle, the potentials and charges of all capacitive meshes are linked together through a system of N linear equations of

$$\Phi_i = \sum_n pp_{i,n}Q_n, \text{ for } i = 1\ldots N \tag{14}$$

where N is the number of capacitive meshes and the coefficient of potential between two capacitive meshes (i and n) is defined as

$$pp_{i,n} = \frac{1}{a_i a_n}\iint (G_{\phi,\mathrm{SP}} + G_{\phi,\mathrm{SW}})ds'_n ds_i. \tag{15}$$

Conventionally, under the (quasi-)static condition, one may assume $pp_{i,n}$'s are all real numbers and invert (14) to obtain the shorted-circuit capacitance matrix. Since $pp_{i,n}$ is, in general, a complex number for dynamic problems, this procedure will result in a complex capacitance matrix. Such a direct inversion indeed violates the conventional definition of capacitance.

Adopting the concept of a generalized inductance recently proposed, this nonconformance issue is overcome by extracting only the (quasi-)static portion of (15) for calculating the shorted-circuit capacitance matrix (which is now complied with the definition of capacitance) and moving its frequency-dependent portion to the inductance matrix. It is, mathematically, done by separating $G_{\phi,\mathrm{SP}}$ into two parts as

$$\begin{aligned} G^0_{\phi,\mathrm{SP}} &= G_{\phi 0} \text{ with } k_0 \to 0 \\ G^f_{\phi,\mathrm{SP}} &= G_{\phi,\mathrm{SP}} - G^0_{\phi,\mathrm{SP}}, \end{aligned} \tag{16}$$

where $G_{\phi 0}$ is the inverse Hankel transform of (7b) or (11). This treatment then leads to

$$\begin{aligned} pp_{i,n} = pp^0_{i,n} + pp^f_{i,n} &= \frac{1}{a_i a_n} \iint G^0_{\phi,\mathrm{SP}} ds'_n ds_i \\ &+ \frac{1}{a_i a_n} \iint \left(G^f_{\phi,\mathrm{SP}} + G_{\phi,\mathrm{SW}} \right) ds'_n ds_i. \end{aligned} \tag{17}$$

The first integral in (17) is the (quasi-)static definition for the coefficients of potential from which the real-valued shorted-circuit capacitances can be obtained. Hence, one can generate the capacitive portion of the equivalent circuit as usual. On the other hand, the frequency-dependent second integral is not used for obtaining the capacitive network but rather is used for generating the inductive matrix.

D. Generalized Complex Inductance

From (3) and (4), the mutual inductance between two inductive meshes (l and m) or self-inductance ($l = m$) is given by

$$L_{l,m} = \frac{1}{w_l w_m} \iint \left(G^{xx}_{A,\mathrm{SP}} + G^{xx}_{A,\mathrm{SW}} \right) ds'_m ds_l. \tag{18}$$

Again, it is generally a complex number. As there is no matrix inversion involved here, the imaginary part does produce a physically meaningful self-resistance ($l = m$). Now, by absorbing the second integral in (17) into the inductance term (18), a generalized self- and mutual inductance is formed. The resulting generalized inductance becomes (see Fig. 2)

$$\bar{L}_{l,m} = L_{l,m} + \frac{pp^{f+}_{l,n_1}}{\omega^2} - \frac{pp^{f-}_{l,n_1}}{\omega^2} - \frac{pp^{f+}_{l,n_2}}{\omega^2} + \frac{pp^{f-}_{l,n_2}}{\omega^2}. \tag{19}$$

The significance of introducing such generalized inductance is that it not only correctly accounts for the radiation effect, but also preserves the physical meaning of the capacitance matrix. Notice that the generalized self-inductance ($l = m$) should always have a negative imaginary part. However, for the generalized mutual inductance, the sign depends on the reference directions of current in the two relevant inductive elements.

III. Short Dipole on Microstrip Substrate

From the classic antenna theory, it is known that a short dipole of length l in free-space has an equivalent radiation resistance of $80\pi^2(l/\lambda)^2$. Now, let us take a look of how the idea of generalized inductance can be used to analyze the radiation resistance for a short dipole on microstrip substrate. Referring to the PEEC model for a single inductive cell as shown in Fig. 3, when the conductive loss is omitted, the following equation can be obtained from (4):

$$j\omega L I + (pp^+_+ - pp^-_+)Q^+ + (pp^+_- - pp^-_-)Q^- = 0. \tag{20}$$

Considering the current continuity equation that $-j\omega Q^+ = -I$ and $-j\omega Q^- = I$, (20) can be rewritten as

$$\begin{aligned} j\omega \left[L - \frac{1}{\omega^2} \left(pp^{f+}_+ - pp^{f-}_+ - pp^{f+}_- + pp^{f-}_- \right) \right] I \\ + \left(pp^{0+}_+ - pp^{0-}_+ \right) Q^+ + \left(pp^{0+}_- - pp^{0-}_- \right) Q^- = 0. \end{aligned} \tag{21}$$

The term inside the square brackets is defined as the generalized complex self-inductance $\bar{L}$, for which, the imaginary part (multiplied by $j\omega$) represents the overall radiation resistance of the small dipole. Following the discussion on Green's functions above, the radiation resistance

$$\mathrm{Re}\{j\omega\bar{L}\}_{\mathrm{org}} = \frac{\eta k_0^2 l^2}{4\pi} - \frac{\eta k_0^2 l^2}{12\pi} = \frac{\eta k_0^2 l^2}{6\pi} \tag{22a}$$

$$\begin{aligned} \mathrm{Re}\{j\omega\bar{L}\}_{\mathrm{img}} = &-\frac{\eta k_0^2 l^2}{4\pi} \left(\frac{\sin \bar{k}_0}{\bar{k}_0} \right) - \frac{K \eta k_0^2 l^2}{12\pi} \\ &- \frac{\eta}{2\pi} \sum_n K^{n-1}(K^2 - 1) \\ &\times \left(\frac{\sin n\bar{k}_0}{n\bar{k}_0} - \frac{\sin n\bar{k}_0 f_n}{n\bar{k}_0 f_n} \right) \end{aligned} \tag{22b}$$

$$\begin{aligned} \mathrm{Re}\{j\omega\bar{L}\}_{\mathrm{sfw}} = &\frac{\eta k_0^2 l^2}{4\pi} \sum_i \pi \mathrm{Res}^A_i \frac{k_{\rho i}}{k_0} \left(k^2_{\rho i} - k_0^2 \right)^{-1/2} \\ &- \frac{\eta k_0^2 l^2}{8\pi} \sum_n \pi \mathrm{Res}^\phi_n \frac{k^3_{\rho n}}{k_0^3} \left(k^2_{\rho n} - k_0^2 \right)^{-1/2} \end{aligned} \tag{22c}$$

$$\begin{aligned} \mathrm{Re}\{j\omega\bar{L}\}_{\mathrm{hoe}} = &-\frac{\eta k_0^2 l^2}{4\pi} \mathrm{Im} \left\{ \frac{g^{xx}_A(\rho)_{\rho=0}}{k_0} \right\} \\ &+ \frac{\eta}{2\pi} \mathrm{Im} \left\{ \frac{g_\phi(\rho)_{\rho=0} - g_\phi(\rho)_{\rho=l}}{k_0} \right\}. \end{aligned} \tag{22d}$$

can be decomposed into four components including the original free-space term (R_{org}), the term due to quasi-static images (R_{img}), the surface-wave term (R_{sfw}), and the remaining term contributed by lateral waves and other higher-order effects (R_{hoe}). After a lengthy derivation, it can be shown that the real part of $j\omega\bar{L}$ is given, in terms of these four components, by (22). Notice that η is the free-space intrinsic impedance, $\bar{k}_0 = k_0 \cdot 2h$

$$f_n = \sqrt{1 + \left(\frac{l}{n \cdot 2h} \right)^2}, n = 1, 2, \ldots, \tag{23}$$

and

$$\frac{\mu_0}{4\pi} g^{xx}_A(\rho) = \int \frac{F^{xx}_A k_\rho}{j2k_{z0}} H^{(2)}_0(k_\rho \rho) dk_\rho \tag{24a}$$

$$\frac{1}{4\pi\varepsilon_0} g_\phi(\rho) = \int \frac{F_\phi k_\rho}{j2k_{z0}} H^{(2)}_0(k_\rho \rho) dk_\rho. \tag{24b}$$

A few interesting features can been seen from the above derived results. Firstly, when $\varepsilon_r = 1$, both (22c) and (22d) are equal to zero. In addition, (22b) reduces to

$$\begin{aligned} \mathrm{Re}\{j\omega\bar{L}\}_{\mathrm{img}} = &-\frac{\eta k_0^2 l^2}{4\pi} \left(\frac{\sin \bar{k}_0}{\bar{k}_0} \right) \\ &+ \frac{\eta}{2\pi} \left(\frac{\sin \bar{k}_0}{\bar{k}_0} - \frac{\sin \bar{k}_0 f_1}{\bar{k}_0 f_1} \right). \end{aligned} \tag{25}$$

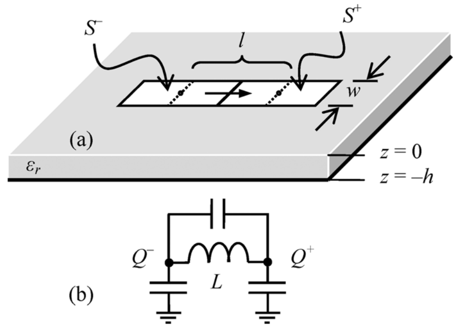

Fig. 3. Short dipole on microstrip substrate, (a) physical configuration; and (b) equivalent circuit.

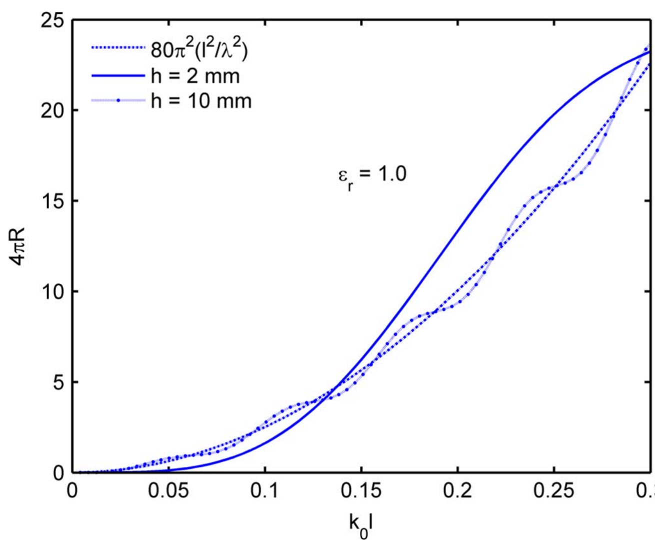

Fig. 4. Radiation resistance of a short dipole over an infinite ground plane.

Fig. 4 shows the plots of total radiation resistance versus $k_0 l$ for two such cases with $h = 2$ mm and $h = 10$ mm. It is clearly seen that the resistance is "oscillatory" proportional to$k_0^2 l^2$ because of the sinc functions in (25) and it reduces, as expected, to the value of $80\pi^2(l/\lambda)^2$ when h increases towards infinity. Secondly, for $\varepsilon_r > 1$, all types of radiation come into existence. In this case, power losses due to surface waves, lateral waves and other higher-order effects will influence the total resistance. Fig. 5(a) and (b) show the cases of $\varepsilon_r = 2.33$, $h = 2$ mm and $h = 4$ mm. It can be seen from the figure that, for the $h = 2$ mm case, there is a sudden jump in the surface waves when $k_0 l$ reaches $\sim$0.13. At this point, the component $(R_{\text{total}} - R_{sfw})$ represents the power radiated into free-space drops significantly. For comparison, the free-space (R_{org}) and total (R_{total}) radiation resistances are also plotted in these figures. A similar feature can be seen for the case of $h = 4$ mm, in which the power radiated into free-space drops every time when a new surface wave mode starts propagating.

In order to have a more general picture of these radiation components, h is increased to 10 mm and the corresponding resistance values are shown in Fig. 5(c). Here, the ripples of the radiation resistance for surface waves converge towards the asymptotic curve, which corresponds to the power radiated towards the dielectric half-space in the case of $h \to \infty$. At the

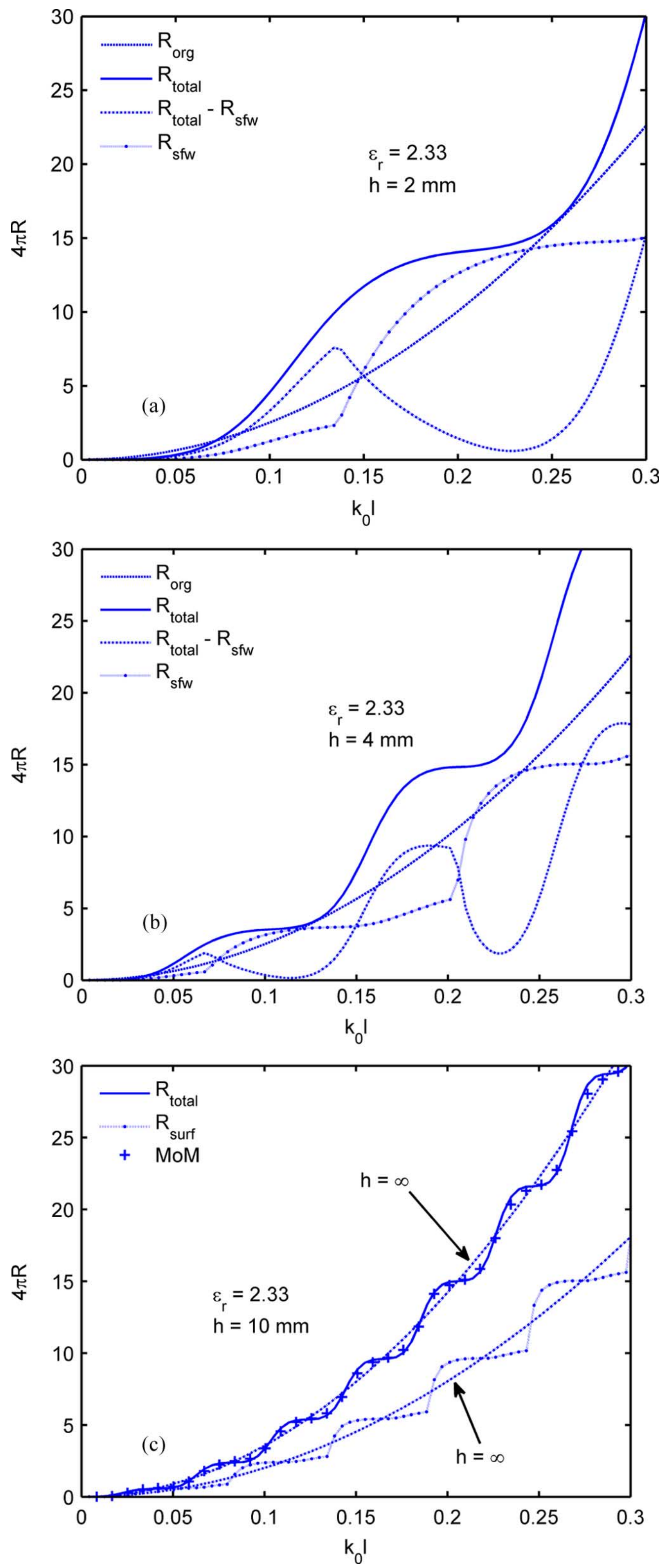

Fig. 5. Radiation resistance components of a short dipole on microstrip substrate, (a) $h = 2$ mm, (b) $h = 4$ mm; and (c) $h = 10$ mm.

same time, the total radiation resistance grows "approximately" along $\sqrt{(\varepsilon_r + 1)}/\sqrt{2}$ times of the free-space dipole resistance. This value corresponds to the sum of the power radiated into the air half-space and into the dielectric half-space under the quasi-static assumption in which lateral waves and other higher-

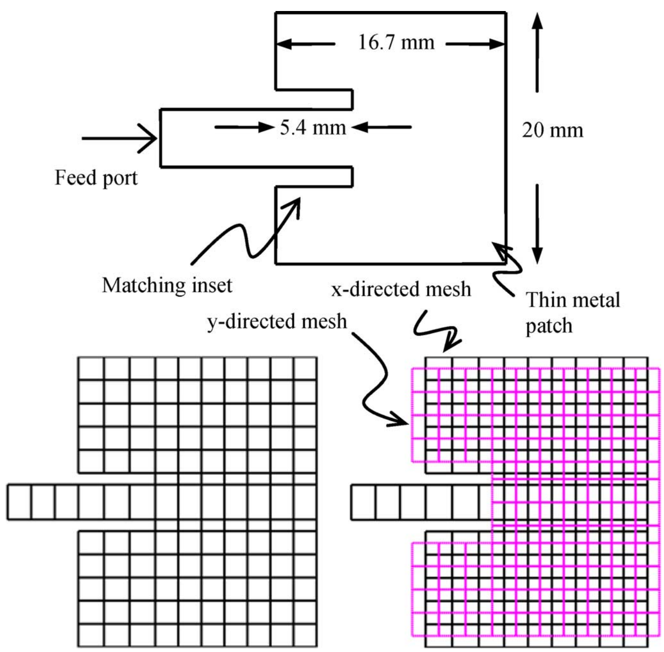

Fig. 6. Geometry for the patch antenna with negligible surface waves.

order effects are ignored. In addition, the total radiation resistance obtained using a commercial MoM solver is plotted also in Fig. 5(c) for comparison.

IV. Numerical Examples

A. Patch Antenna on Thin Substrate

The first example to be studied is a patch antenna on thin substrate. The substrate used in this example has a dielectric constant of 2.33 and a thickness of 0.787 mm. As the substrate is thin and has a small value of dielectric constant, the surface-wave contributions to the Green's functions are relatively insignificant at low frequencies. This can be verified from the small residue value (Res^{ϕ}) for the (only) pole of $\tilde{G}_{\phi}$. The size of the patch antenna (see Fig. 6) is 16.7 mm × 20 mm. It is fed by a microstrip with an inset of 5.4 mm to match to a 50-Ω transmission line. The geometry is divided into a total of 127 capacitive meshes and 222 inductive meshes, corresponding to a meshing scheme of ~30 meshes per (free-space) wavelength at 6.2 GHz. These meshes are shown in Fig. 6 for reference. Notice that there are two types of inductive mesh, one is x-directed and one is y-directed. From the simulated results in Fig. 7, it is seen that the patch operates at around 5.8 GHz. The scattering parameters calculated by the proposed PEEC-based model agree well with those from a MoM-based commercial EM solver.

B. Thin-Strip Dipole on Microstrip Substrate

The second example is a thin-strip dipole on a microstrip substrate of thickness 1.575 mm and dielectric constant 2.33. The surface wave portion of the electric scalar Green's function in this case is significant. The geometry of the dipole is depicted in Fig. 8. It comprises of two infinitely thin metal strips of 2.1 mm in length and 0.2 mm in width. The dipole is excited at the center by a lumped power port of 50 Ω. A simplified equivalent circuit when the structure is divided into eight capacitive meshes is also

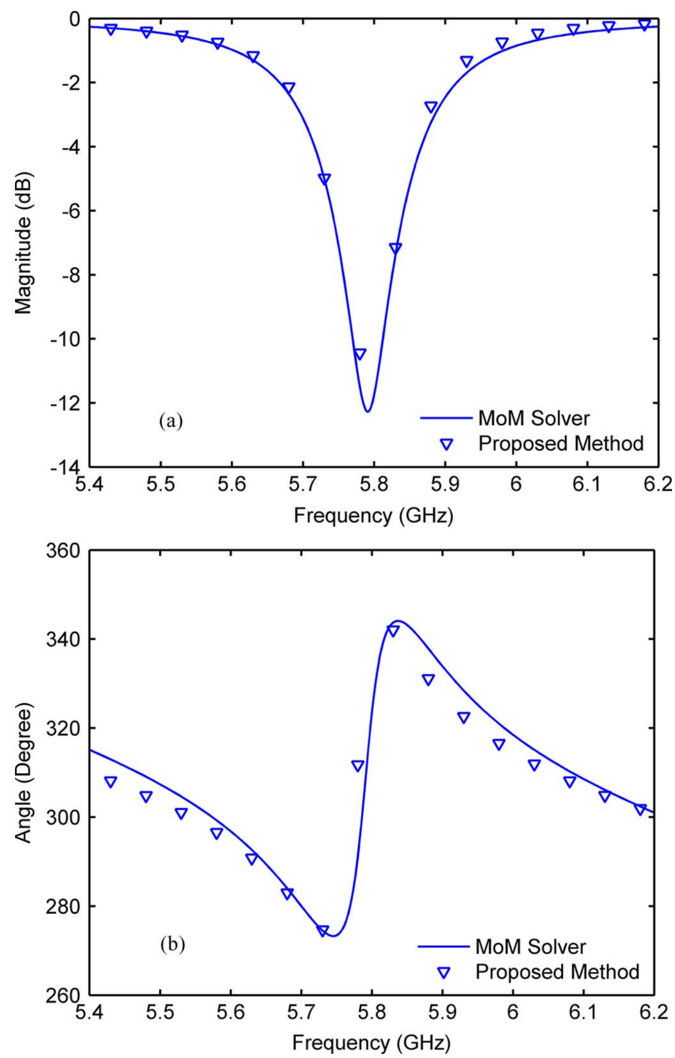

Fig. 7. Simulated results (S_{11}) for the patch antenna with negligible surface waves, (a) magnitude; and (b) phase angle.

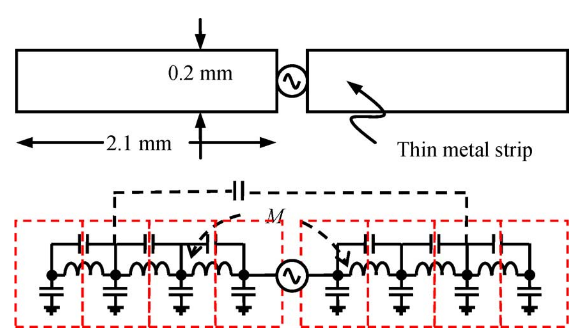

Fig. 8. Geometry for the thin-strip dipole and its simplified eight-capacitive-mesh equivalent circuit (not all mutual components are shown).

shown in the figure. Notice that not all mutual capacitances and inductances are shown in the circuit for clarity. In the proposed PEEC formulation, the thin dipole is divided into 36 capacitive meshes and 34 inductive meshes, corresponding to a scheme of 100 meshes per (free-space) wavelength at 26 GHz. Simulated scattering parameters from a commercial full-wave solver and those from the proposed PEEC model are depicted in Fig. 9. It is seen from the figure that the dipole exhibits a series resonant at

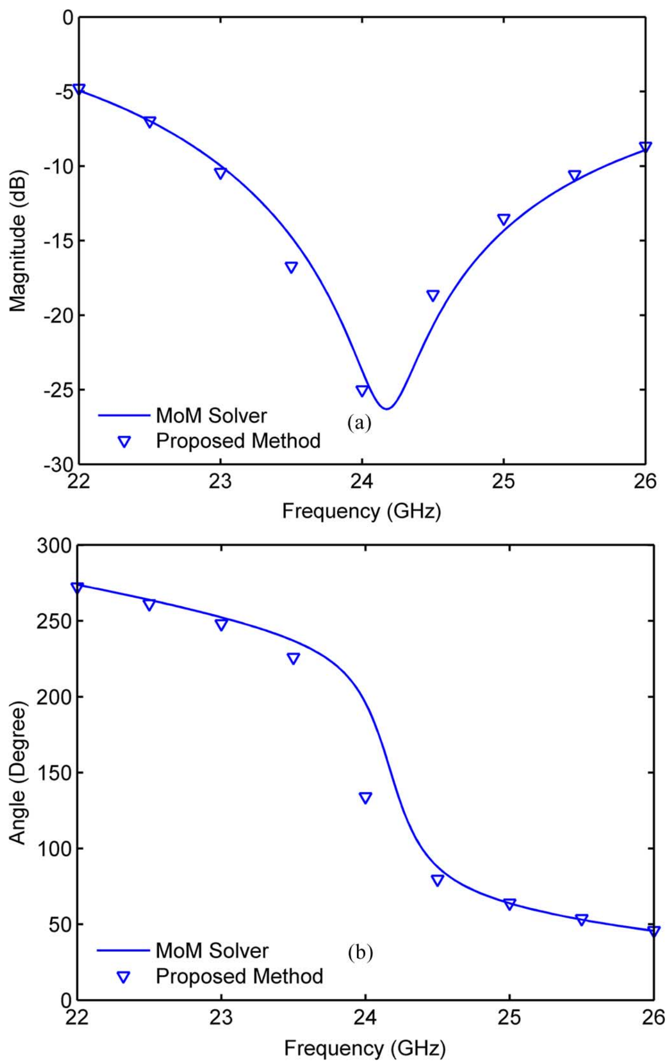

Fig. 9. Simulated results (S_{11}) for the thin-strip dipole, (a) magnitude; and (b) phase angle.

around 24 GHz, and acts as a half-wave dipole at this particular frequency as expected. Since the basis functions and meshing schemes for the two models are different, some discrepancies can be seen from the two sets of S_{11}. Such small discrepancies are reasonable among different full-wave EM models.

V. Conclusion

A new PEEC formulation, which incorporates the concept of generalized complex inductance, for modeling of microstrip structures has been introduced. In this PEEC formulation, the radiation loss is taken into account accurately by having complex-valued inductors in the equivalent circuit. And through these inductors, contributions from various radiation mechanisms, such as spatial and surface waves, to the overall radiation are revealed. Numerical examples, which include a patch antenna with negligible surface waves and a thin-strip dipole on microstrip substrate, have been studied. It is seen from these examples that equivalent circuit models having generalized complex-valued inductors can correctly account for the radiation loss in terms of "distributed" frequency-dependent resistances.

References

[1] A. Ruehli, "Equivalent circuit models for three dimensional multi-conductor systems," *IEEE Trans. Microw. Theory Tech.*, vol. 22, no. 3, pp. 216–221, Mar. 1974.

[2] H. Heeb and A. Ruehli, "Three-dimensional interconnect analysis using partial element equivalent circuits," *IEEE Trans. Circuits Syst.*, vol. 39, no. 11, pp. 974–982, Nov. 1992.

[3] A. Ruehli, "Circuit models for three-dimensional geometries including dielectrics," *IEEE Trans. Microw. Theory Tech.*, vol. 40, no. 7, pp. 1507–1516, Jul. 1992.

[4] H. Shi, J. Fan, and J. Drewniak, "Modeling multilayered PCB power-bus designs using an MPIE based circuit extraction technique," in *Proc. IEEE Int. Symp. EMC*, Denver, 1998, pp. 647–651.

[5] L. Chang and K. Chang, "Accurate and efficient inductance extraction for SoC noise and signal integrity," in *Proc. IEEE Int. Conf. Electrical Perf. Electronic Packag. Conf. Rec,*, 2002, pp. 209–213.

[6] B. Archambeault, "Analyzing power/ground plane decoupling performance using the partial element equivalent circuit (PEEC) simulation technique," in *Proc. IEEE Int. Symp. EMC*, Washington, DC, 2000, pp. 779–784.

[7] S. A. Teo, B. L. Ooi, S. T. Chew, and M. S. Leon, "A fast PEEC technique for full-wave parameters extraction of distributed elements," *IEEE Microw. Wireless Compon. Lett.*, vol. 11, no. 5, pp. 226–228, May 2001.

[8] K.-L. Wu, L. K. Yeung, and Y. Ding, "An efficient PEEC algorithm for modeling of LTCC RF circuits with finite metal strip thickness," *IEEE Microw. Wireless Compon. Lett.*, vol. 13, no. 9, pp. 390–392, Sep. 2003.

[9] V. Vahrenholt, H. Brüns, and H. Singer, "Fast EMC analysis of systems consisting of PCBs and metallic antenna structures by a hybridization of PEEC and MoM," *IEEE Trans. Electromagn. Compat.*, vol. 52, no. 11, pp. 962–973, Nov. 2010.

[10] J. Garrett, A. Ruehli, and C. Paul, "Accuracy and stability improvements of integral equation models using the partial element equivalent circuit (PEEC) approach," *IEEE Trans. Antennas Propagat.*, vol. 46, no. 12, pp. 1824–1832, Dec. 1998.

[11] A. Ruehli *et al.*, "Nonorthogonal PEC formulation for time- and frequency-domain EM and circuit modeling," *IEEE Trans. Electromagn. Compat.*, vol. 45, no. 5, pp. 167–176, May 2003.

[12] S. Kochetov and G. Wollenberg, "Stability of full-wave PEEC models: Reason for instabilities and approach for correction," *IEEE Trans. Electromagn. Compat.*, vol. 47, no. 11, pp. 738–748, Nov. 2005.

[13] X. Zhang and Z. Feng, "A new retarded PEEC model for antenna," presented at the IEEE Asia-Pacific Microwave Conf., Hong Kong.

[14] S. Sundberg and J. Ekman, "PEEC modeling of antenna characteristics," in *Proc. IEEE Int. Symp. EMC*, Portland, OR, 2006, pp. 580–585.

[15] L. K. Yeung and K.-L. Wu, "Generalized partial element equivalent circuit (PEEC) modeling with radiation effect," *IEEE Trans. Microw. Theory Tech.*, vol. 59, no. 10, pp. 2377–2384, Oct. 2011.

[16] S. V. Kochetov, G. Wollenberg, and M. Leone, "Peec-models based on dyadic Green's functions for structures in layered media," in *Proc. IEEE Int. Symp. EMC EME*, 2007, pp. 179–182.

[17] F. Ling, D. Jiao, and J. Jin, "Efficient electromagnetic modeling of microstrip structures in multilayer media," *IEEE Trans. Microw. Theory Tech.*, vol. 47, no. 9, pp. 1810–1818, Sep. 1999.

[18] A. Torabian and Y. Chow, "Simulated image method for Green's function of multilayer media," *IEEE Trans. Microw. Theory Tech.*, vol. 47, no. 9, pp. 1777–1781, Sep. 1999.

[19] E. Karabulut, A. Erdogan, and M. Aksun, "Discrete complex image method with automatic order selection," *IEEE Trans. Microw. Theory Tech.*, vol. 59, no. 10, pp. 2385–2393, Oct. 2011.

[20] A. Alparslan, M. Aksun, and K. Michalski, "Closed-form Green's functions in planar layered media for all ranges and materials," *IEEE Trans. Microw. Theory Tech.*, vol. 58, no. 3, pp. 602–613, Mar. 2010.

[21] S. Teo, S. Chew, and M. Leong, "Error analysis of the discrete complex image method and pole extraction," *IEEE Trans. Microw. Theory Tech.*, vol. 51, no. 2, pp. 406–413, Feb. 2003.

[22] F. Mesa, R. Boix, and F. Medina, "Closed-form expressions of multilayered planar Green's functions that account for the continuous spectrum in the far field," *IEEE Trans. Microw. Theory Tech.*, vol. 56, no. 7, pp. 1601–1614, Jul. 2008.

[23] Y. Chow, J. Yang, D. Fang, and G. Howard, "A closed-form spatial Green's function for the thick microstrip substrate," *IEEE Trans. Microw. Theory Tech.*, vol. 39, no. 7, pp. 588–592, Jul. 1991.

Lap K. Yeung (S'00–M'02) received the B.Eng. degree in electrical and information engineering from University of Sydney, Sydney, Australia, in 1998, the M.Eng. degree in electronic engineering from The Chinese University of Hong Kong, Shatin, Hong Kong, in 2002, and the Ph.D. degree in electrical engineering from University of California at Los Angeles, Los Angeles, CA, in 2009.

During 1999, he was with the Commonwealth Scientific and Industrial Research Organization (CSIRO), Sydney, Australia, where he was a research engineer involved in the numerical modeling of different antenna structures. From 2003 to 2006, he was with The Chinese University of Hong Kong, where he is involved in various LTCC multichip-module (MCM) designs and the development of numerical algorithms for analyzing multilayer embedded RF modules.

Ke-Li Wu (M'90–SM'96–F'11) received the B.S. and M.Eng. degrees from the Nanjing University of Science and Technology, Nanjing, China, in 1982 and 1985, respectively, and the Ph.D. degree from Laval University, Quebec, QC, Canada, in 1989.

From 1989 to 1993, he was with the Communications Research Laboratory, McMaster University, as a Research Engineer and a Group Manager. In March 1993, he joined the Corporate Research and Development Division, COM DEV International, the largest Canadian space equipment manufacturer, where he was a Principal Member of Technical Staff. Since October 1999, he has been with The Chinese University of Hong Kong, Shatin, Hong Kong, where he is currently a Professor and the Director of the Radio frequency Radiation Research Laboratory (R3L). He has authored or coauthored numerous publications in the areas of EM modeling and microwave passive components, microwave filters and antenna engineering. His current research interests include partial element equivalent circuit (PEEC) and derived physically expressive circuit (DPEC) EM modeling of high-speed circuits, RF and microwave passive circuits and systems, synthesis theory and practices of microwave filters, antennas for wireless terminals, LTCC-based multichip modules (MCMs), and RF identification (RFID) technologies. His research group is the main workforce in various active RFID research and applications in Hong Kong.